Nucleon Energy Correlators

Xiaohui Liu*
Center of Advanced Quantum Studies, Department of Physics, Beijing Normal University, Beijing, 100875, China and Center for High Energy Physics, Peking University, Beijing 100871, China

Hua Xing Zhu†
Zhejiang Institute of Modern Physics, Department of Physics, Zhejiang University, Hangzhou, 310027, China

(Received 13 September 2022; revised 13 December 2022; accepted 3 February 2023; published 27 February 2023)

We introduce the concept of the nucleon energy correlators, a set of novel objects that encode the microscopic details of a nucleon, such as the parton angular distribution in a nucleon, the collinear splitting to all orders, as well as the internal transverse dynamics of the nucleon. The nucleon energy correlators complement the conventional nucleon or nucleus tomography, but without introducing the nonperturbative fragmentation functions or the jet clustering algorithms. We demonstrate how the nucleon energy correlators can be measured in the lepton-nucleon deep inelastic scattering. The predicted distributions display a fascinating phase transition between the perturbative and nonperturbative regime. In the perturbative phase, a polar angle version of the Bjorken scaling behavior is predicted. We discuss its possible applications and expect it to aggrandize the physics content at the electron ion colliders with a far-forward detector.

DOI: 10.1103/PhysRevLett.130.091901

Introduction.—The femtoscale structure of the nucleon has been the central scientific importance of nuclear physics for decades. The next generation QCD facilities [1–3] will boost the revelation of the nucleon and nucleus partonic structure in great detail. The conventional approach to the nucleon and nucleus tomography is to probe its transverse momentum dependent (TMD) structure functions through either the semi-inclusive deep inelastic scattering (SIDIS) [4–9] or the jet-based studies [10–25]. However SIDIS calls for the knowledge of the TMD fragmentation functions, while jets involve the clustering procedure and require high machine energy, either probes seem to complicate the analysis in one way or another.

There are other substitutions to jets and identified hadrons, such as event-shape observables and the energy-energy correlator (EEC) [26,27]. Recently, there have been ongoing efforts to reformulate jet substructure physics using the EEC and its higher point generalization [28]. This is largely inspired by the unprecedented detector resolution at the LHC, as well as insights from conformal collider physics [29–34]. For recent application of energy correlators in jet substructure see, for example, [35–49].

The EEC measures the correlation $\langle \mathcal{E}(n_i)\mathcal{E}(n_j)\rangle$ between the energy deposit in two detectors along directions n_i and n_j with angular separation θ_{ij}, where $\mathcal{E}(n) = \lim_{r\to\infty}\int_0^\infty dt T_{0\vec{n}}(t,\vec{n}r)r^2$ is the asymptotic energy flow operator with $T_{\mu\nu}$ the energy-stress tensor [50–53]. One particular interesting feature of the EEC is its collinear limit as $\theta_{ij}\to 0$, in which the EEC exhibits a universal scaling behavior (modulo running coupling effects), $\lim_{n_j\to n_i}\mathcal{E}(n_i)\mathcal{E}(n_j)\sim\theta^{\gamma(\alpha_s)}$ as described by the light-ray OPE [29,32]. The collinear limit is well encoded in the EEC jet function [34]

$$J^q_{EEC}(\theta^2) = \sum_X\sum_{i,j\in X}\frac{\not{n}_{\alpha\beta}}{2}\langle\Omega|\bar{\chi}_n\delta_{Q,\mathcal{P}_n}\delta(\theta^2-\theta_{ij}^2)|X\rangle_\alpha \times\frac{E_iE_j}{(Q/2)^2}\langle X|\chi_n|\Omega\rangle_\beta, \quad (1)$$

where χ_n is the gauge invariant n-collinear quark field in the soft collinear effective theory (SCET) [54–58] that serves the source to create collinear particles out of the vacuum $|\Omega\rangle$ and Q represents the hard scale that initiates the process. E_i and E_j are the energies measured. The lightlike vectors are $n=(1,\vec{0}_\perp,1)$ and $\bar{n}=(1,\vec{0}_\perp,-1)$. When $\theta Q\gg\Lambda_{\rm QCD}$, the EEC jet function can be predicted using the collinear splitting functions [34,35]. When $\theta Q\sim\Lambda_{\rm QCD}$, a striking confining transition was observed in analyzing CMS Open Data [40].

The EEC has also been adapted to the TMD studies in DIS, where the back-to-back limit $\theta_{ij}\to\pi$ is probed instead [59–61]. It was shown that when the EEC is measured in DIS in this limit, the unpolarized TMD parton

distribution arises [59,61]. However, given that the EEC essentially measures the *final state correlations* and carries no information on the nucleon, the current EEC probe of the TMDs is indirect, in the sense that the EEC is used as a simple replacement of the jets or hadrons, while its power and features are not yet fully exploited.

In this Letter, we propose a novel energy correlator called the nucleon EEC that probes the initial-final state correlation. The nucleon EEC encodes the information on the nucleon three-dimensional microscopic structures, meanwhile inheriting the fascinating features of the conventional final-state EEC. As one of the major results of this work, we will demonstrate the accessibility to the nucleon EEC via the measurement in DIS

$$\Sigma_N(Q^2,\theta^2)=\sum_i\int d\sigma(x_B,Q^2,p_i)x_B^{N-1}\frac{\bar{n}\cdot p_i}{P}\delta(\theta^2-\theta_i^2), \tag{2}$$

where $N\geq 1$ is a positive power and $d\sigma$ is the differential cross section. x_B is the Bjorken variable and θ_i is the polar angle of the calorimeter measured with respect to the beam. p_i denotes the momentum flow into the detector and P the momentum of the incoming nucleon while Q^2 the virtuality of the photon. We leave the detailed explanation to the rest of the Letter.

The nucleon energy-energy-correlator.—We first generalize the EEC jet function to introduce the (unpolarized) nucleon EEC, whose definition is

$$f^q_{\mathrm{EEC}}(N,\theta^2)=\sum_X\sum_{k\in X}\frac{\not{\bar{n}}_{\alpha\beta}}{2}\langle P|\bar{\chi}_n\delta_{z_kP,\mathcal{P}_n}\delta(\theta^2-\theta_k^2)|X\rangle_\alpha \times z_b^{N-1}\frac{\bar{n}\cdot p_k}{P}\langle X|\chi_n|P\rangle_\beta. \tag{3}$$

Here z_b is the partonic momentum fraction with respect to the incoming hadron P that enters the hard interaction at the hard scale Q. Here θ_k is the polar angle of the calorimeter k with respect to the beam. The gluon nucleon EEC can be defined similarly using the gauge invariant gluonic field.

The nucleon EEC correlates the energy E_k from the initial state radiation that flows into the calorimeter and the energy z_b that participates in the hard interaction, as illustrated in Fig. 1. The nucleon EEC has several fascinating features: (i) The nucleon EEC probes the nucleon internal transverse degrees of freedom through the polar angle θ when $\theta\sim\mathcal{O}(\Lambda_{\mathrm{QCD}}/Q)$. It measures the partonic θ distribution within the nucleon induced by the intrinsic transverse dynamics.The nucleon EEC complements the conventional nucleon tomography by using the TMD PDFs. The nucleon EEC evolves as the moment of the collinear PDFs,

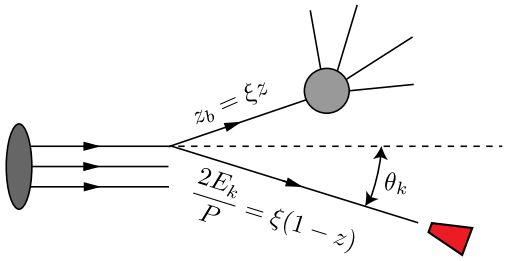

FIG. 1. The momentum flow due to an initial state splitting where a fraction of $z_b=\xi z$ goes into the hard interaction at the scale Q, while the rest, including the remnants contributed when $\theta_k\sim\mathcal{O}(\Lambda_{\mathrm{QCD}}/Q)$, will deposit in the calorimeter.

$$\frac{df^i_{\mathrm{EEC}}(N,\theta^2,\mu)}{d\ln\mu^2}=\gamma^N_{ij}f^j_{\mathrm{EEC}}, \tag{4}$$

where γ^N_{ij} is the Mellin moment of the collinear splitting kernel $\gamma^N_{ij}=\int_0^1 dz\,z^{N-1}P_{ij}(z)$, and i, j are parton flavor indices. Compared with the TMD PDFs, the nucleon EEC is free of the Sudakov suppression, hence it is likely to provide better resolutions to the intrinsic nonperturbative structures. As concrete examples, we will demonstrate the nucleon EEC can be probed in DIS and will also discuss the generalization of the unpolarized EEC in Eq. (3) to the polarized case. (ii) When the transverse momentum $\theta Q\gg\Lambda_{\mathrm{QCD}}$, the nucleon EEC can be factorized into the product of a perturbatively calculable coefficient I_{ij} and the Mellin moment of the collinear PDF $f_{j/P}(N,\mu)=\int_0^1 d\xi\xi^{N-1}f_{j/P}(\xi,\mu)$, which gives

$$f^i_{\mathrm{EEC}}(N,\theta^2,\mu)=I_{ij}(N,\theta^2,\mu)f_{j/P}(N+1,\mu), \tag{5}$$

where I_{ij} encodes the complete information on θ. While the details of I_{ij} remained to be calculated order by order using the collinear splitting function similar to the conventional EEC, its scale dependence is fixed to all orders by

$$\frac{dI_{ij}(N,\theta^2,\mu)}{d\ln\mu^2}=\gamma^N_{ik}I_{kj}-I_{ik}\gamma^{N+1}_{kj}. \tag{6}$$

At the leading logarithmic (LL) accuracy, we thus find the f^i_{EEC} satisfies the scaling behavior

$$f^i_{\mathrm{EEC}}(N,\theta^2,\mu)=\left[e^{\frac{2\gamma^{(0),N}}{\beta_0}L}I^{(0)}(N,\theta^2)e^{-\frac{2\gamma^{(0),N+1}}{\beta_0}L}\right]_{ij}f_{j/P}(N+1,\mu), \tag{7}$$

where $I^{(0)}$ is the leading matching coefficient [62]. $(\alpha_2/2\pi)\gamma^{(0),N}_{ij}$ is the leading order moment of splitting function and $L=\ln[\alpha_s(Q\theta)/\alpha_s(\mu)]$. If $\alpha_s(Q\theta)$ is small enough, the nucleon EEC satisfies the scaling behavior

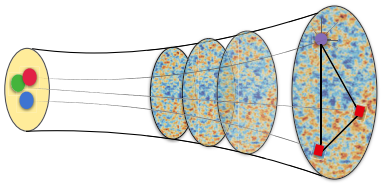

FIG. 2. Nucleon 3-point correlation function.

$f_{\rm EEC} \sim \theta^{-2}\theta^{[\alpha_s(Q)/2\pi]\gamma^{(0),N}}\theta^{-[\alpha_s(Q)/2\pi]\gamma^{(0),N-1}}$. In this sense, the nucleon EEC faithfully probes the initial state collinear splitting in the vacuum through the θ distribution. Deviations from the power-law scaling could shed light on the nature of the initial state source that induces the modification. For example, when the transverse momentum $\theta Q \sim \Lambda_{\rm QCD}$, we expect the nonperturbative structure of the proton becomes important, where a nonperturbative modification is needed in (7), whose detailed study we leave for future work. (iii) The nucleon EEC can be straightforwardly generalized to the multiple energy correlators by measuring the energy $E_1, \ldots, E_n$ deposit in multiple caloremiters with angular separation θ_{ij} with $i, j = 1, \ldots n$ and the beam. The underlying nucleon internal microscopic details will be imprinted in the detailed structure of these correlation functions, see Fig. 2, in analogy with the details of the early universe imprinted in cosmological correlation functions. We will leave detailed studies on the nucleon multi-energy correlation to future works. (iv) In the extreme small angle limit, we expect simple scaling behavior $\sim\theta^2$ for the nucleon EEC, which signifies the existence of a free hadron phase in initial state beam jet. Similar behavior has been seen in the final state jet using CMS open data [40].

The x_B weighted deep-inelastic scattering.—To see how the nucleon EEC can be measured, we consider the DIS process $l + P \to l' + X$ in the frame where the virtual photon γ^* acquires no transverse momentum, e.g., the $\gamma^* - P$ center-of-mass frame or the Breit frame. We assume the nucleon is moving along the $+z$ direction. We measure the Bjorken $x_B = [(-q^2)/(2P \cdot q)]$ and the momentum flow p_i^μ deposit (including the ones from the beam remnants) in a calorimeter along the direction i. Here $q = l' - l$ is the momentum carried by the virtual photon. In this Letter we will be particularly interested in the scenario where the detector is placed in the far-forward region and therefore the transverse momentum flow $p_{i,t}^2 \sim \theta^2 E_i^2$ is very small compared with $q^2 = -Q^2$, as depicted in Fig. 3.

The measurement probes the weighted cross section $\Sigma_N(Q^2, \theta)$ in Eq. (2). We note that the polar angle θ_i is related to the transverse momentum as $\sin\theta_i = (p_{i,t}/E_i)$. For the time being, we assume the proton is unpolarized.

The weighted cross section in Eq. (2) can be calculated via

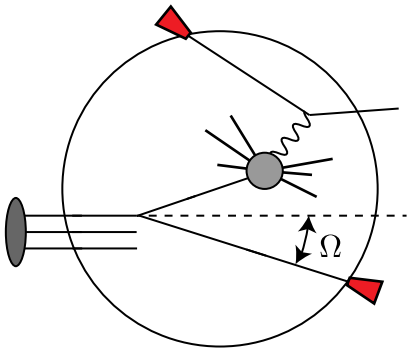

FIG. 3. x_B and p_i measurement in DIS that will probe the nucleon EEC $f_{\rm EEC}$. Here Ω stands for (θ_i, ϕ_i) with ϕ_i the azimuthal angle measured with respect to the nucleon spin.

$$\Sigma_N(Q^2, \theta^2) = \frac{\alpha^2}{Q^4}\int dx_B x_B^{N-1} \sum_{i\in X, \lambda = T,L} e_i^2 f_\lambda(y) \times \int d^4x e^{iq\cdot x}\langle P|j^\dagger \cdot \epsilon_\lambda^* \frac{2\mathcal{E}(\theta)}{P} j \cdot \epsilon_\lambda(x)|P\rangle, \tag{8}$$

where j^μ is the conserved current. ϵ_λ is the virtual photon polarization vector with $\lambda = L, T$ for the longitudinal and transverse polarization, respectively. $f_\lambda(y)$ is the photon flux such that $f_T = 1 - y + y^2/2$ and $f_L = 2(1-y)$ where $y = [(2p\cdot q)/(2p\cdot l)]$ is the inelastcity. We note that the property of the similar matrix element with $|P\rangle$ replaced by the vacuum state has been discussed in context of the conformal collider physics [29].

When $\theta \ll 1$ and thus i is close to the beam, it is ready to show by using SCET [54–58] that Σ_N takes the factorized form at LL

$$\Sigma_N(Q^2, \theta^2) = f_{\rm EEC}^i(N, \theta^2, \mu)\int d\zeta\, \zeta^{N-1}\frac{d^2\hat{\sigma}_i(\mu)}{d\zeta dQ^2} + \mathcal{O}(\theta), \tag{9}$$

where we see the occurrence of the nucleon EEC $f_{\rm EEC}^i(N, \theta)$ and therefore the proposed measurement does probe the nucleon EEC. The z_b^{N-1} within $f_{\rm EEC}^i(N, \theta)$ in Eq. (3) enters through the x_B^{N-1} weight. We note that the coefficient of $f_{\rm EEC}^i$ is nothing but the Mellin-moment $d\hat{\sigma}_i(N, \mu)$ of the partonic DIS cross section [71], satisfying $d\hat{\sigma}_i(N,\mu)/d\ln\mu^2 = -\gamma_{ij}^N\hat{\sigma}_j(N,\mu)$. Here i and j can either be a quark or a gluon.

When $\theta Q \gg \Lambda_{\rm QCD}$, the nucleon EEC is further factorized following Eq. (5). Thus the scale dependence of the coefficient I_{ij} in Eq. (6) is an immediate consequence of the scale independence of the weighted cross section $d\Sigma_N/d\ln\mu = 0$.

Now we estimate the requirement of the forward detector for this measurement. Suppose we want to probe the

intrinsic transverse momentum of the nucleon, we will demand the detector to detect transverse momentum flow $p_{i,t} \sim \Lambda_{\rm QCD}$ and thus to cover polar angles down to $\theta \sim p_{i,t}/Q$. Hence for $Q \sim \mathcal{O}(5\ {\rm GeV})$, the estimated $\theta \sim \mathcal{O}(0.2\ {\rm rad})$, which is well covered by the EIC far-forward particle detection plan [1,2,65,66] and will be even better favored if the coverage proposals such as the Zero Degree Calorimeter [65,67] down to and below 5 mrad would be realized. We emphasize that since we only count the energy deposit in the calorimeters, no jet clustering procedure is needed. Meanwhile, instead of using the calorimetry, the track-based measurements can be carried out [28,38,39] to offer better pointing and angular resolution.

Here we predict the normalized differential distribution $\langle {\rm EEC} \rangle_N = 1/\sigma \theta^2 d\Sigma_N(\theta^2)$ in the Breit frame. We define the rapidity $y = \ln \tan \theta/2$. For the prediction, we use `Pythia82` [68] with the proton $P = 275$ GeV and the incoming lepton $l = 10$ GeV.

In Fig. 4, we show the predictions for $\langle {\rm EEC} \rangle \equiv \langle {\rm EEC} \rangle_2$, i.e., with $N = 2$. We vary the values of Q with $Q > 10$, $Q > 30$, and $Q > 50$ GeV. We see from the upper panel of Fig. 4 that although the Q's are different, the predicted $\langle {\rm EEC} \rangle$s display similar features, which implies that the normalized distributions reflect the property of the nucleon itself at different scales $\mu \sim Q$.

We note that Fig. 4 exhibits an interesting "phase transition" between the perturbative-phase for $\theta \gtrsim 0.2$ rad and the "free-particle-phase" for $\theta \lesssim 0.005$ rad, connected by the nonperturbative transition region. In the perturbative region, the distribution is almost flat, largely independent of Q's, which is a direct manifestation of Bjorken scaling in the space of polar angle (rapidity), as can be seen from Eq. (7).

The feature is more evident by looking at the slope γ showed in the lower panel of Fig. 4, where in the perturbative region $\gamma \sim 0$, while in the deep nonperturbative region for $\theta \lesssim 0.005$ rad, $\gamma \sim 2$. It will be very interesting if we can confirm such phase transition at future experimental facilities.

We again notice that all the slope γ distributions with different values of Q shares similar behaviour which indicates it reveals the intrinsic property of the nucleon EEC at different scales μ. The transition region moves to the right as we decrease Q, which is expected since the transition occurs when $\theta \sim \mathcal{O}(\Lambda_{\rm QCD}/Q)$. The γ in the perturbative region can be predicted using the LL result in Eq. (7) and the factorization in Eq. (9), which is shown by the red line. All the Q values are covered within the band, obtained by a dramatic variation of μ, from $\mu = 50$ GeV to $\mu = 300$ MeV. We find good agreement between the `Pythia` simulations and the analytic LL result in the perturbative phase. We emphasize that future observed deviation from the predicted slope could be used to extract the nature of the initial state source that induces the modification to the collinear splitting kernel, such as the hadronization and the hot or cold nucleus medium effects. The theory precision can be further improved and we leave it to future works.

In Fig. 5, we show the $\langle {\rm EEC} \rangle_N$ for different N. The smaller values of the N increase the sensitivity to

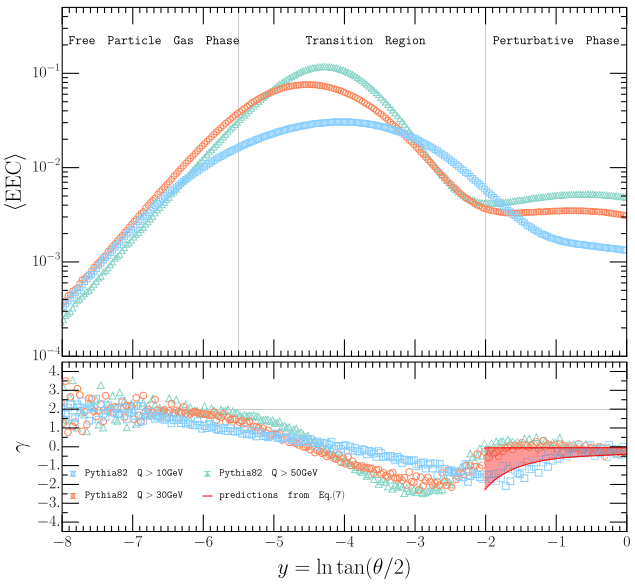

FIG. 4. $\langle {\rm EEC} \rangle$ and γ distribution in the Breit frame.

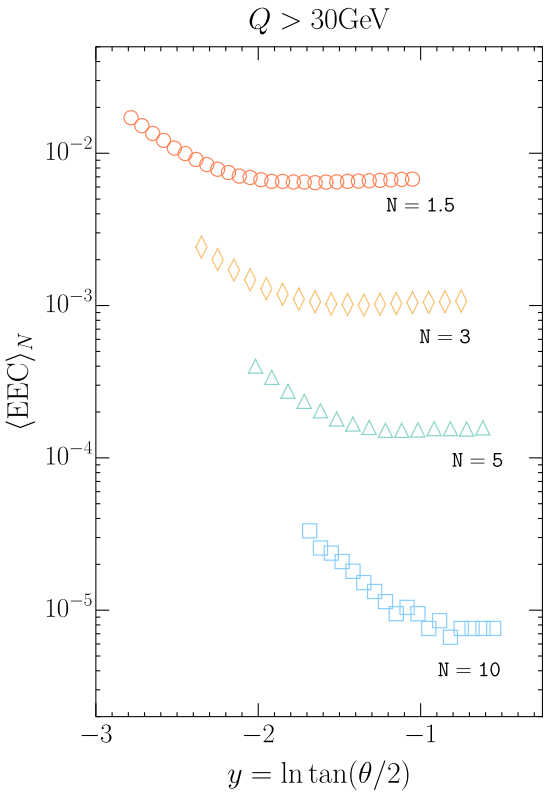

FIG. 5. The angular "Bjorken scaling rule" of the nucleon EEC.

the small-x component of a nucleon while larger N probes more into the large x regime. Again the plot manifests the polar angle (rapidity) scaling behavior of the nucleon EEC, similar to the famous Bjorken scaling rule of the PDFs. We note that for larger N, therefore effectively larger x closer to 1, the transition region appears at larger angle, consistent with the expectation that $\theta \sim \mathcal{O}(\Lambda_{\rm QCD}/Q)$ increase as Q decrease. Also since the normalization of nucleon EEC is propotional to the moment of PDFs, we expect to see a decrease in the magnitude as N increases, as a result of small-x enhancement of PDFs.

Transversely polarized EEC.—Once the incoming nucleon is polarized, we can also probe the spin asymmetry by measuring the azimuthal modulation. Here the beam and the out-going lepton span the x-z plane.

For instance, for the transversely polarized nucleon beam, if we measure the $\sin(\phi - \phi_S)$ distribution with $\phi - \phi_S$ the azimuthal angle between the detector and the nucleon spin, we are probing the spin-dependent distribution $d\Sigma_N(\vec{n}_t, S_T)$ whose $\sin(\phi - \phi_S)$ dependent part factorized similarly as the unpolarized case in Eq. (9), with the replacement of $f^i_{\rm EEC}(\theta)$ by

$$\begin{aligned}&\frac{-\epsilon_T^{ab} n_t^a S_T^b}{M_P} f^q_{T,\rm EEC}(N,\theta)\\ &= \sum_X \sum_{i\in X} z_b^{N-1} \frac{\bar{n}\cdot p_i}{P} \frac{\not{\bar{n}}_{\alpha\beta}}{2}\\ &\quad \times \langle P, S_T|\bar{\chi}_n \delta_{z_i P, \mathcal{P}_n} \delta^{(2)}(\vec{\hat{n}}_t - \vec{\hat{n}}_{i,t})|X\rangle_\alpha \langle X|\chi_n|P,S_T\rangle_\beta,\end{aligned} \tag{10}$$

for quark, where $\vec{n}_t = \sin\theta(\cos\phi, \sin\phi)$, S_T is the nucleon spin and M_P is the nucleon mass. The nonvanishing of $f_{T,\rm EEC}$ is owing to the same mechanism that gives rise to the Sivers effect [69,70]. The Sivers-like EEC $f_{T,\rm EEC}$ induces the $\sin(\phi - \phi_S)$ azimuthal asymmetry $A_N = \{[d\Sigma_N(S_T) - d\Sigma_N(-S_T)]/[\Sigma(S_T) + \Sigma(-S_T)]\}$. The predicion of A_N relies on the nonperturbative input of the $f_{T,\rm EEC}$ which requires further studies in the future. Since there is no Sudakov suppression, we anticipate a better chance to observe the asymmetry at the EIC.

Conclusion.—In this Letter, we introduced the nucleon energy-energy-correlator that measures the correlation of the energy flows from the initial nucleon. The nucleon EEC reflects the parton angular distribution in a nucleon. This new object is novel both theoretically and phenomenologically. Theoretically, we have demonstrated that the microscopic details of the nucleon such as the faithful vacuum collinear splitting behavior as well as the nucleon internal transverse momentum and spin degrees of freedom are imprinted in the energy correlation function, and meanwhile the nucleon EEC may offer additional possibilities to understand the nucleon structures using the light-ray OPE in QCD. Phenomenologically, we showed how the nucleon EEC can be probed at EIC with a far-forward detector. We have set the theoretical foundation for the observable and predict the measured distribution at EIC to exhibit power law scaling behaviors. A novel phase transition between the free-particle and the perturbative phases is observed. In the perturbative region, the polar angle (rapidity) version of the Bjorken scaling behavior is also predicted.

One advantage of the nucleon EEC is that its measurement involves no jet clustering procedure nor additional nonperturbative object other than the nucleon EEC itself. Besides, the factorization in Eq. (9) only involves a product instead of a convolution, and should make the extraction of the nucleon EEC a lot easier. Therefore it serves a clean complement to the conventional TMDs to the nucleon structures, good for either high energy or low energy machines.

Other than the scenarios considered in the Letter, we expect the proposed nucleon EEC to have a wide application to future nucleon or nucleus studies. Extensions to other observables sensitive to the various TMD distributions will follow straightforwardly. By suitably choosing the weight N, the nucleon EEC can be made sensitive to the small-x phenomenology. The nucleon EEC can also be used to study the cold nuclear effect in eA collisions or to extract the hot medium effect with heavy ion data. All these effects will leave a footprint in the deviations from the $\langle {\rm EEC}\rangle_N$ and its slope introduced in this work. As long as one charm is tagged in the detected forward event, the nucleon EEC can offer a direct look into the intrinsic charm content. Furthermore, the generalization of the EEC to multiple point correlations will allow for more delicate differentiation of the nucleon and nucleus microscopic details. We thus anticipate that the nucleon EEC introduced in this work will stimulate further theoretical developments along these directions.

We are grateful to Miguel Arratia, Hao Chen, Zhong-bo Kang, Ian Moult, Jinlong Zhang, and Jian Zhou for insightful discussions. We are grateful for the hospitality of the committee for the "Heavy flavor and QCD" workshop held in Changsha where this work was initiated. We appreciate stimulating feedback from the EicC bi-week meeting. This work is supported by the Natural Science Foundation of China under Contract No. 12175016 (X. L.), No. 11975200 (H. X. Z.), and No. 12147103 (H. X. Z.).

*xiliu@bnu.edu.cn
†zhuhx@zju.edu.cn

[1] R. Abdul Khalek *et al.*, Nucl. Phys. **A1026**, 122447 (2022).
[2] *Proceedings, Probing Nucleons and Nuclei in High Energy Collisions: Dedicated to the Physics of the Electron Ion Collider: Seattle (WA), United States, 2018* (World Scientific Press, Singapore, 2020).
[3] D. P. Anderle *et al.*, Front. Phys. **16**, 64701 (2021).

[4] J. C. Collins, A. V. Efremov, K. Goeke, S. Menzel, A. Metz, and P. Schweitzer, Phys. Rev. D **73**, 014021 (2006).
[5] W. Vogelsang and F. Yuan, Phys. Rev. D **72**, 054028 (2005).
[6] A. Airapetian *et al.* (HERMES Collaboration), Phys. Rev. Lett. **103**, 152002 (2009).
[7] A. Bacchetta and M. Radici, Phys. Rev. Lett. **107**, 212001 (2011).
[8] M. G. Echevarria, A. Idilbi, Z.-B. Kang, and I. Vitev, Phys. Rev. D **89**, 074013 (2014).
[9] I. Scimemi and A. Vladimirov, J. High Energy Phys. 06 (2020) 137.
[10] D. Gutierrez-Reyes, I. Scimemi, W. J. Waalewijn, and L. Zoppi, Phys. Rev. Lett. **121**, 162001 (2018).
[11] X. Liu, F. Ringer, W. Vogelsang, and F. Yuan, Phys. Rev. Lett. **122**, 192003 (2019).
[12] D. Gutierrez-Reyes, Y. Makris, V. Vaidya, I. Scimemi, and L. Zoppi, J. High Energy Phys. 08 (2019) 161.
[13] D. Gutierrez-Reyes, I. Scimemi, W. J. Waalewijn, and L. Zoppi, J. High Energy Phys. 10 (2019) 031.
[14] M. Arratia, Z.-B. Kang, A. Prokudin, and F. Ringer, Phys. Rev. D **102**, 074015 (2020).
[15] X. Liu, F. Ringer, W. Vogelsang, and F. Yuan, Phys. Rev. D **102**, 094022 (2020).
[16] M. Arratia, Y. Makris, D. Neill, F. Ringer, and N. Sato, Phys. Rev. D **104**, 034005 (2021).
[17] H. T. Li and I. Vitev, Phys. Rev. Lett. **126**, 252001 (2021).
[18] Z.-B. Kang, X. Liu, S. Mantry, and D. Y. Shao, Phys. Rev. Lett. **125**, 242003 (2020).
[19] H1, V. Andreev *et al.*, Phys. Rev. Lett. **128**, 132002 (2022).
[20] Z.-B. Kang, J. Terry, A. Vossen, Q. Xu, and J. Zhang, Phys. Rev. D **105**, 094033 (2022).
[21] X. Liu and H. Xing, arXiv:2104.03328.
[22] Z.-B. Kang, K. Lee, D. Y. Shao, and F. Zhao, J. High Energy Phys. 11 (2021) 005.
[23] H. T. Li, Z. L. Liu, and I. Vitev, Phys. Lett. B **827**, 137007 (2022).
[24] W. K. Lai, X. Liu, M. Wang, and H. Xing, arXiv:2205.04570.
[25] Z.-B. Kang, K. Lee, D. Y. Shao, and F. Zhao, J. Phys. Soc. Jpn. Conf. Proc. **37**, 020128 (2022).
[26] C. Basham, L. S. Brown, S. D. Ellis, and S. T. Love, Phys. Rev. Lett. **41**, 1585 (1978).
[27] C. Basham, L. Brown, S. Ellis, and S. Love, Phys. Rev. D **19**, 2018 (1979).
[28] H. Chen, I. Moult, X. Zhang, and H. X. Zhu, Phys. Rev. D **102**, 054012 (2020).
[29] D. M. Hofman and J. Maldacena, J. High Energy Phys. 05 (2008) 012.
[30] A. Belitsky, S. Hohenegger, G. Korchemsky, E. Sokatchev, and A. Zhiboedov, Phys. Rev. Lett. **112**, 071601 (2014).
[31] A. Belitsky, S. Hohenegger, G. Korchemsky, E. Sokatchev, and A. Zhiboedov, Nucl. Phys. **B884**, 305 (2014).
[32] M. Kologlu, P. Kravchuk, D. Simmons-Duffin, and A. Zhiboedov, J. High Energy Phys. 01 (2021) 128.
[33] G. Korchemsky, J. High Energy Phys. 01 (2020) 008.
[34] L. J. Dixon, I. Moult, and H. X. Zhu, Phys. Rev. D **100**, 014009 (2019).
[35] H. Chen, M.-X. Luo, I. Moult, T.-Z. Yang, X. Zhang, and H. X. Zhu, J. High Energy Phys. 08 (2020) 028.
[36] H. Chen, I. Moult, and H. X. Zhu, Phys. Rev. Lett. **126**, 112003 (2021).
[37] C.-H. Chang, M. Kologlu, P. Kravchuk, D. Simmons-Duffin, and A. Zhiboedov, J. High Energy Phys. 05 (2022) 059.
[38] Y. Li, I. Moult, S. S. van Velzen, W. J. Waalewijn, and H. X. Zhu, Phys. Rev. Lett. **128**, 182001 (2022).
[39] M. Jaarsma, Y. Li, I. Moult, W. Waalewijn, and H. X. Zhu, J. High Energy Phys. 06 (2022) 139.
[40] P. T. Komiske, I. Moult, J. Thaler, and H. X. Zhu, Phys. Rev. Lett. **130**, 051901 (2023).
[41] J. Holguin, I. Moult, A. Pathak, and M. Procura, arXiv:2201.08393.
[42] K. Yan and X. Zhang, Phys. Rev. Lett. **129**, 021602 (2022).
[43] H. Chen, I. Moult, J. Sandor, and H. X. Zhu, J. High Energy Phys. 09 (2022) 199.
[44] C.-H. Chang and D. Simmons-Duffin, arXiv:2202.04090.
[45] H. Chen, I. Moult, J. Thaler, and H. X. Zhu, J. High Energy Phys. 07 (2022) 146.
[46] K. Lee, B. Meçaj, and I. Moult, arXiv:2205.03414.
[47] A. J. Larkoski, arXiv:2205.12375.
[48] L. Ricci and M. Riembau, Phys. Rev. D **106**, 114010 (2022).
[49] T.-Z. Yang and X. Zhang, J. High Energy Phys. 09 (2022) 006.
[50] N. A. Sveshnikov and F. V. Tkachov, Phys. Lett. B **382**, 403 (1996).
[51] F. V. Tkachov, Int. J. Mod. Phys. A **12**, 5411 (1997).
[52] G. P. Korchemsky and G. F. Sterman, Nucl. Phys. **B555**, 335 (1999).
[53] C. W. Bauer, S. P. Fleming, C. Lee, and G. F. Sterman, Phys. Rev. D **78**, 034027 (2008).
[54] C. W. Bauer, S. Fleming, D. Pirjol, and I. W. Stewart, Phys. Rev. D **63**, 114020 (2001).
[55] C. W. Bauer, D. Pirjol, and I. W. Stewart, Phys. Rev. D **65**, 054022 (2002).
[56] C. W. Bauer and I. W. Stewart, Phys. Lett. B **516**, 134 (2001).
[57] M. Beneke, A. P. Chapovsky, M. Diehl, and T. Feldmann, Nucl. Phys. **B643**, 431 (2002).
[58] C. W. Bauer, S. Fleming, D. Pirjol, I. Z. Rothstein, and I. W. Stewart, Phys. Rev. D **66**, 014017 (2002).
[59] H. T. Li, I. Vitev, and Y. J. Zhu, J. High Energy Phys. 11 (2020) 051.
[60] A. Ali, G. Li, W. Wang, and Z.-P. Xing, Eur. Phys. J. C **80**, 1096 (2020).
[61] H. T. Li, Y. Makris, and I. Vitev, Phys. Rev. D **103**, 094005 (2021).
[62] See Supplemental Material at http://link.aps.org/supplemental/10.1103/PhysRevLett.130.091901 for the exemplary derivation of the matching coefficient, which includes Refs [63,64].
[63] H. Cao, X. Liu, and H. X. Zhu (to be published).
[64] I. W. Stewart, F. J. Tackmann, and W. J. Waalewijn, J. High Energy Phys. 09 (2010) 005.
[65] M. Arratia *et al.*, Nucl. Instrum. Methods Phys. Res., Sect. A **1047**, 167866 (2023) (2022).
[66] D. Cebra, X. Dong, Y. Ji, S. R. Klein, and Z. Sweger, Phys. Rev. C **106**, 015204 (2022).
[67] A. Bylinkin *et al.*, arXiv:2208.14575.

[68] T. Sjöstrand, S. Ask, J. R. Christiansen, R. Corke, N. Desai, P. Ilten, S. Mrenna, S. Prestel, C. O. Rasmussen, and P. Z. Skands, Comput. Phys. Commun. **191**, 159 (2015).
[69] D. W. Sivers, Phys. Rev. D **41**, 83 (1990).
[70] J. C. Collins, Phys. Lett. B **536**, 43 (2002).

[71] Strictly speaking, this is only true if we integrate x_B down to 0 in Eq. (2). However, if we choose sufficiently large N, to suppress the contribution from the small values of x_B, the integral will be well approximated by the Mellin moment.